

## An Alternative Reaction Pathway for Iridium Catalyzed Water Oxidation Driven by CAN

Alberto Bucci, Gabriel Menendez Rodriguez, Gianfranco Bellachioma, Cristiano Zuccaccia, Albert Poater, Luigi Cavallo, and Alceo Macchioni

*ACS Catal.*, **Just Accepted Manuscript** • DOI: 10.1021/acscatal.6b01325 • Publication Date (Web): 10 Jun 2016

Downloaded from <http://pubs.acs.org> on June 14, 2016

### Just Accepted

“Just Accepted” manuscripts have been peer-reviewed and accepted for publication. They are posted online prior to technical editing, formatting for publication and author proofing. The American Chemical Society provides “Just Accepted” as a free service to the research community to expedite the dissemination of scientific material as soon as possible after acceptance. “Just Accepted” manuscripts appear in full in PDF format accompanied by an HTML abstract. “Just Accepted” manuscripts have been fully peer reviewed, but should not be considered the official version of record. They are accessible to all readers and citable by the Digital Object Identifier (DOI®). “Just Accepted” is an optional service offered to authors. Therefore, the “Just Accepted” Web site may not include all articles that will be published in the journal. After a manuscript is technically edited and formatted, it will be removed from the “Just Accepted” Web site and published as an ASAP article. Note that technical editing may introduce minor changes to the manuscript text and/or graphics which could affect content, and all legal disclaimers and ethical guidelines that apply to the journal pertain. ACS cannot be held responsible for errors or consequences arising from the use of information contained in these “Just Accepted” manuscripts.



# An Alternative Reaction Pathway for Iridium Catalyzed Water Oxidation Driven by CAN

Alberto Bucci,<sup>a</sup> Gabriel Menendez Rodriguez,<sup>a</sup> Gianfranco Bellachioma,<sup>a</sup> Cristiano Zuccaccia,<sup>a</sup> Albert Poater,<sup>b</sup> Luigi Cavallo,<sup>c\*</sup> and Alceo Macchioni<sup>a\*</sup>

<sup>a</sup>Department of Chemistry, Biology and Biotechnology, University of Perugia and CIRCC, Via Elce di sotto, 8, I-06123 Perugia, Italy. <sup>b</sup>Institut de Química Computacional i Catàlisi and Departament de Química, Universitat de Girona, Campus Montilivi, 17071 Girona, Catalonia, Spain. <sup>c</sup>King Abdullah University of Science and Technology (KAUST), KAUST Catalysis Center (KCC), Thuwal 23955-6900, Saudi Arabia

Supporting Information Placeholder

**ABSTRACT:** The generation of solar fuels by means of a photosynthetic apparatus strongly relies on the development of an efficient water oxidation catalyst (WOC). Cerium ammonium nitrate (CAN) is the most commonly used sacrificial oxidant to explore the potentiality of WOCs. It is usually assumed that CAN has the unique role to oxidatively energize WOCs, making them capable to offer a low energy reaction pathway to transform H<sub>2</sub>O to O<sub>2</sub>. Herein we show that CAN might have a much more relevant and direct role in WO, mainly related to the capture and liberation of O–O containing molecular moieties.

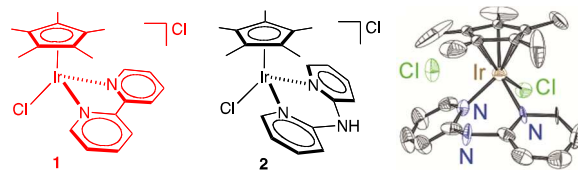
**KEYWORDS:** *water oxidation, iridium complexes, cerium ammonium nitrate, reaction mechanism, DFT calculations*

Water Oxidation (WO) to molecular oxygen is one of the most important chemical reactions because the protons and electrons that are liberated might be exploited to produce solar fuels.<sup>1,2</sup> Due to kinetic concerns, a catalyst (C)<sup>3,4</sup> is necessary to lower and level, as more as possible, the energetic of the oxidative steps. Unless C acts also as photosensitizer and electron/hole separating agent, whatever the nature of C is, WOC must be preliminarily “energized” by an oxidant in order to make it capable to promote WO. In Nature, this occurs through the interaction of the oxygen-evolving complex with the radical tyrosine (generated from P680<sup>+</sup> and imidazole of His 190 *via* a PCET process).<sup>5</sup> In a man-made apparatus, oxidation takes place by the interaction of WOC with either a properly selected chemical oxidant,<sup>6</sup> an anode (photoelectrochemical catalysis),<sup>7</sup> or a photo-oxidant derived from the interaction of light with a photosensitizer (photocatalysis).<sup>8</sup> As a consequence, the knowledge of the WOC/oxidant interaction mechanism is of primary importance but, rather surprisingly, such an issue is little faced<sup>9,10,11,12,13,14,15</sup> in the astonishingly increasing number of papers dealing with WOCs.

During our attempts<sup>16</sup> to develop new and better performing WOCs based on iridium,<sup>17</sup> we decided to explore the potential of an organometallic compound formally derived from the insertion of a –NH– electron donating bridge between the two pyridine rings of the previously reported [Cp\*Ir(bpy)Cl]Cl WOC (**1**; bpy = 2,2'-bipyridine, Scheme 1).<sup>16a</sup> The rationale is twofold and aims at favoring the oxidative steps and assisting remov-

al of protons from a water molecule coordinated at iridium center.

Herein we show that the new [Cp\*Ir(dpa)Cl]Cl WOC (**2**; dpa = 2,2'-dipyridylamine, Scheme 1) is indeed much more active than **1** when catalysis is driven by CAN (Cerium Ammonium Nitrate) but, more importantly, it exhibits a peculiar catalytic behavior when a relative little excess (80–320 equivalents) of CAN is used. Particularly, CAN is always consumed faster than O<sub>2</sub> evolution and, in extreme cases, it is almost completely consumed before O<sub>2</sub> starts to be formed. An in-depth kinetic investigation, paralleled by quantum mechanical calculations, led to suggest an alternative reaction pathway in which, after CAN-driven and iridium catalyzed O–O bond formation, O<sub>2</sub> is slowly liberated through an uncatalyzed process, likely from a cerium intermediate species.



**Scheme 1.** Left: Sketch of **1** and **2** WOCs. Right: ORTEP view of complex **2**. Ellipsoids are drawn at the 50% probability level. Selected bond distances (Å) and angles (deg): Ir–N1 = 2.121(12), Ir–N3 = 2.133(12), Ir–Cl1 = 2.392(4), Ir–Cp\* = 1.788; N1–Ir–N3 = 82.96(4), N1–Ir–Cl1 = 88.8(3), N3–Ir–Cl1 = 87.9(3), Cp\*–Ir–N1 = 130.3, Cp\*–Ir–N3 = 125.5, Cp\*–Ir–Cl1 = 127.2. Cp\* is the centroid of the C11, C12, C13, C14 and C15 atoms.

Complex **2** was synthesized by the reaction of the dimeric precursor [Cp\*IrCl<sub>2</sub>]<sub>2</sub> with 2 equivalents of dpa in methylene chloride at room temperature (SI). **2** was completely characterized in solution by multinuclear and

multidimensional NMR spectroscopy and in the solid state by X-Ray crystallography (Scheme 1 and SI).

Complexes **1** and **2** were tested as WOCs using CAN as sacrificial oxidant. It was found that the catalytic behaviors of **1** and **2** are markedly different. In particular, the activity of complex **2** is strongly dependent on the molar ratio between CAN and catalyst ( $R = [\text{CAN}]/[\text{C}]$ ), whereas that of **1** is little sensitive to such a ratio (Figure 1, left). In experiments in which  $[\text{CAN}] = 10 \text{ mM}$ , TOF of **2** reaches a maximum of  $38 \text{ min}^{-1}$  when  $[\text{C}] = 15.6 \text{ }\mu\text{M}$  and  $R = 640$  (Figure 1, left). Furthermore, the trends of oxygen evolution with **2** show an increase of activity at the end of the run. For instance, when  $[\text{CAN}] = 5 \text{ mM}$  and  $[\text{C}] = 5 \text{ }\mu\text{M}$  ( $R = 1000$ ), the TOF *versus*  $t$  trends indicate that initially **1** and **2** have a similar TOF but that of **2** increases up to a maximum value ( $25 \text{ min}^{-1}$ ), close to the end of the catalytic run, more than 6 times higher than that of **1** ( $4 \text{ min}^{-1}$ ), which remains substantially constant until the end of catalysis (Figure 1, right). Previous studies on the oxidative transformations of IrCp\*–precursors for WO clearly indicate that many active species can be generated, potentially having different catalytic activity.<sup>16b,18,19,20</sup> Furthermore, very recently, Reek and coworkers showed that the nature of the ancillary ligand(s) attached to IrCp\*–moiety strongly affects the activation and catalysis of the resulting complexes.<sup>21</sup> <sup>1</sup>H NMR experiments in which **1** and **2** were reacted with 80 equivalents of CAN (10 mM) revealed a higher tendency of the latter to undergo Cp\*–oxidative transformation, as judged from the amount of acid acetic formed (41% for **2** and 25% for **1**, Figures S9 and S10). The introduction of a peripheral –NH moiety might be responsible for the easier oxidative degradation of **2** generating more active sites, in analogy with what elegantly demonstrated by Fukuzumi for 4,4'–OH disubstituted bpy.<sup>22</sup>

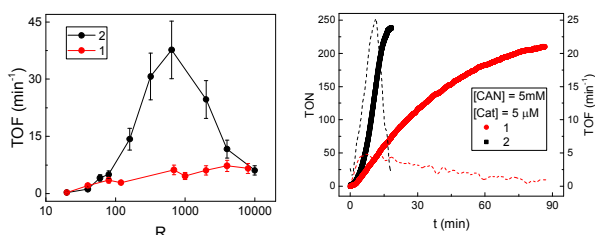


**Figure 1.** (Left) Trends of TOF versus  $R$  for **1** and **2** WOCs obtained by means of differential manometry ( $R$  scale is log). (Right) Comparison of TON (continuous line) and TOF (dashed line) versus  $t$  of **1** and **2** WOCs under exactly the same experimental conditions.

The kinetics of WO with **1** and **2** was studied more in details approaching the problem by independently following the disappearance of CAN by UV-Vis spectroscopy, evaluated at 390 nm, and the evolution of  $\text{O}_2$  by manometry and Clark electrode. All experiments were performed at  $[\text{CAN}] = 5\text{--}10 \text{ mM}$  whereas  $[\text{C}]$  was increased to reach the desired low  $R$  values. Having fixed the concentration of CAN at such high values ensured that the amount of evolved oxygen was accurately detected.

A peculiar behavior was found for both catalysts at low  $R$  values (80–320) where the rate of CAN consumption was always higher than that of  $\text{O}_2$  evolution for both

WOCs, even though this phenomenon is much more accentuated for **2** (compare Figures S12–S14 with Figures S15–S17). As an example, for the latter, CAN consumption is perfectly accompanied by  $\text{O}_2$  evolution when  $R = 2000$  (Figure 2, left), with the two trends crossing at almost exactly half of the expected cycles (250); instead, when  $R = 80$ , all CAN is consumed in less than two minutes, whereas  $\text{O}_2$  evolution starts just slightly before two minutes, reaching a plateau after about eight minutes (Figure 2, right). To verify that the lower rate of  $\text{O}_2$  production was correctly evaluated by differential manometry, experiments were repeated following  $\text{O}_2$  production by Clark electrode in solution; exactly the same results were obtained in terms of induction time and rate of  $\text{O}_2$  evolution (Figure S18). A similar marked difference in the velocity of CAN consumption with respect to  $\text{O}_2$  evolution was observed in all runs of multiple addition experiments (Figure S19), even if the overlapping between the two trends slightly increases with number of runs.

Although part of CAN equivalents was surely consumed for oxidatively transforming the precatalysts, this cannot account for all consumption of CAN, otherwise no oxygen evolution should be observed. Furthermore, the discrepancy between CAN consumption and  $\text{O}_2$  production should be much more limited, or absent, in runs successive to the first one and this is not the case (Figure S19).

In order to explore the generality of higher rate for CAN consumption with respect to  $\text{O}_2$  evolution, we performed analogous kinetic experiments also for  $[\text{Cp}^*\text{Ir}(\text{bzipy})(\text{NO}_3)]\text{NO}_3$  (**3**) and  $[\text{Cp}^*\text{Ir}(\text{H}_2\text{O})_3](\text{NO}_3)_2$  (**4**), two well-established WOCs, and  $\text{IrO}_2$  (**5**), the benchmark heterogeneous WOC. It was found that CAN depletion was always faster than  $\text{O}_2$  evolution, even if for **1**, **3** and **5** WOCs, which were the slowest catalysts under our conditions, the phenomenon was less accentuated (Figure S24–S33). Also for **4**, experiments of multiple additions of CAN show that CAN consumption was complete before  $\text{O}_2$  production for cycles successive to the first one, analogously to what observed for **2** (Figure S34). Interestingly, a comparison of the two multiple-run experiments for **2** and **4** shows that CAN consumption is much faster for the latter, whereas  $\text{O}_2$  evolution substantially occurs with the same rate in all runs (Figure S35).

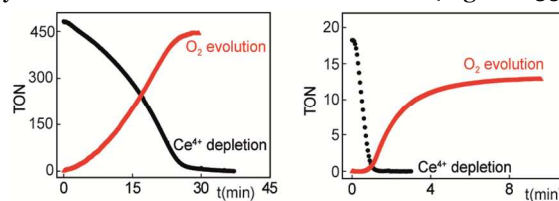


**Figure 2.** Kinetic trends of CAN depletion and  $\text{O}_2$  evolution for **2** WOC measured by UV-Vis and differential manometer when  $R = 2000$  (left) and  $R = 80$  (right) ( $[\text{CAN}] = 10 \text{ mM}$ ).

The observations reported above clearly point toward the formation of an intermediate (X), which accumulates in between  $\text{Ce}^{\text{IV}}$  and  $\text{O}_2$ . For those reasons we treated our data using the simplest kinetic model, typical of a three species consecutive reaction, involving the reaction of  $\text{Ce}^{\text{IV}}$  to afford X ( $k_1^{\text{obs}}$ ) followed by the liberation of  $\text{O}_2$  from X ( $k_2^{\text{obs}}$ ) (SI). Clearly, C might intervene in each re-

action; consequently,  $k_1^{\text{obs}}=k_1[\text{C}]^n$  and  $k_2^{\text{obs}}=k_2[\text{C}]^m$ , where  $n$  and  $m$  are the reaction orders of  $\text{C}$ , respectively.  $k_1^{\text{obs}}$  and  $k_2^{\text{obs}}$  were derived fitting the kinetic trends with  $[\text{Ce}^{\text{IV}}]=[\text{Ce}^{\text{IV}}]_0-4k_1^{\text{obs}}t$  and  $[\text{O}_2]=[\text{Ce}^{\text{IV}}]_0/4\{1-\exp(-k_2^{\text{obs}}t)\}$ , respectively (Figures S35 and S36).  $k_1^{\text{obs}}$  and  $k_2^{\text{obs}}$  data for **1** and **2** and other WOCs are reported in the SI. From the dependence of  $k_1^{\text{obs}}$  and  $k_2^{\text{obs}}$  on  $[\text{C}]$ , the orders  $n$  and  $m$  on the catalyst were calculated. Interestingly, it was found that  $n \approx 1$  and  $m \approx 0$  for all catalysts, indicating that the role of catalyst is exerted only in reaction leading to  $\text{X}$ , which is the fastest under our conditions of little  $R$  values, whereas evolution of  $\text{O}_2$  from  $\text{X}$  seems to be an uncatalyzed reaction determining the global reaction rate. Consistently, when  $[\text{C}]$  is decreased, down to the typical values exploited in standard catalytic experiments (1–5  $\mu\text{M}$ ), depletion of  $\text{Ce}^{\text{IV}}$  becomes the rate determining step and the trends of  $\text{Ce}^{\text{IV}}$  consumption and  $\text{O}_2$  evolution are perfectly coherent and cross at exactly midpoint (Figure 2).

As far as the nature of  $\text{X}$  is concerned, several scenarios might be envisioned considering that  $\text{X}$  must have the capability of releasing  $\text{O}_2$ . As stated above, it is unlikely that an oxidized form of iridium WOCs uniquely constitutes  $\text{X}$ , also because the maximum TON reachable in cases as that reported in Figure 2 would be 1.

Another possibility is that  $\text{X} = \text{H}_2\text{O}_2$ . However, also this hypothesis is unlikely for several reasons. First of all, it is well known that CAN quickly reacts with  $\text{H}_2\text{O}_2$  thus making little probable its accumulation during WO reactions.<sup>23</sup> Consistently, we performed some kinetic experiments between CAN (10 mM) and  $\text{H}_2\text{O}_2$  (5 mM) under conditions analogous to those used for WO. Indeed, we found that reaction is much faster than WO catalysis ( $k_{\text{CAN}}^{\text{obs}}=99.5$  mM/min and  $k_{\text{O}_2}^{\text{obs}}=73.0$  mM/min, Figure S38). Secondly, we performed some kinetic experiments of  $\text{H}_2\text{O}_2$  disproportionation in the presence of WOC and  $\text{Ce}^{\text{III}}$ , under the absurdum assumption that all CAN is consumed to quantitatively generate  $\text{H}_2\text{O}_2$  (Figure S39). The reaction did not occur at all in the timescale of WO reaction. These experiments exclude the possibility that  $\text{X} = \text{H}_2\text{O}_2$ .

A hypothesis that agrees with all observations is that  $\text{X}$  is a Ce species, containing an O–O moiety, capable of releasing  $\text{O}_2$  without the intervention of the catalyst. The formation of such a species is a viable possibility since polynuclear cerium compounds bearing both  $\mu$ - and  $\mu$ - $\eta^2$ : $\eta^2$ -peroxo bridging<sup>24,25,26,27</sup> as well as monohydroperoxide species of cerium<sup>28,29</sup> are well documented in the literature. In this respect, very recently, Tsurugi and Mashima showed that a stable and well-characterized  $\mu$ - $\eta^2$ : $\eta^2$ -peroxo bridged-Ce(IV) dimer easily form from the reaction of a monomeric Ce(III) precursor and dissolved  $\text{O}_2$ .<sup>30</sup> Furthermore, the affinity of ceria for reactive oxygen species (ROS) is very well known;<sup>31</sup> as a matter of fact it is frequently used as free-radical scavenger with important applications in medicine, biology, energy and catalysis.<sup>31</sup>

In order to shed some light on the nature of  $\text{X}$ , multiple run UV-Vis experiments with **2** ( $R = 80$ ) were carefully analyzed. A band at 570 nm was found to have the correct kinetic features of an intermediate: it grows during CAN depletion, with a similar rate constant, reaching a maximum of intensity when CAN is finished,

and disappears during  $\text{O}_2$  evolution, again with a similar rate constant, in all runs (Figure S19). Although a similar band has been observed before and has been assigned to molecular  $\text{Ir}(\text{IV})$ <sup>32</sup> and clusters/nanoparticles of  $\text{Ir}$ ,<sup>33</sup> it is also consistent with the formation of a Ce(IV) dimer analogous to that reported by Tsurugi and Mashima,<sup>30</sup> which shows a band at 575 nm. None of two possibilities can be proved or discarded with certainty; nevertheless, the latter appears to be slightly preferable because it better agrees with the non-synchronous CAN depletion and un-catalyzed  $\text{O}_2$  evolution. This would mean that, at low  $R$  values, Ce(IV) has not the necessary potential to induce the last oxidative step<sup>34</sup> and, during such an attempt, likely occurring through an inner sphere mechanism, a moiety containing the preformed O–O unit is transferred from  $\text{Ir}$  to a Ce dimer (or cluster<sup>35</sup>), which evolves  $\text{O}_2$  without the intervention of  $\text{Ir}$ . Consistently, such behavior is expected and found to be more accentuated for catalysts having a higher tendency to enter the catalytic cycle as **2** and **4** for which the real  $R$  coincides with the nominal one.<sup>34</sup> It is important to outline that no hypothesis has been done on the nature of the iridium active species that can consequently be just the molecular precursor, a still molecular oxidized derivative or even an aggregate of nanometric dimensions.<sup>22,33,36</sup>

With the aim of rationalizing the kinetic results we performed DFT calculations for **2**,<sup>37</sup> focusing on O–O bond formation involving both  $\text{Ir}$  and Ce species. Considering that the mechanism of O–O bond formation in  $\text{Ir}$  organometallic WOCs and the structure of CAN in solution are still matter of debate, the only scope of this section is to show that a low energy pathway for O–O bond formation involving Ce species is viable. To limit the number of assumptions, we considered species already proposed in literature by Sakai and others,<sup>9,11,12</sup> namely  $\text{L}_n\text{Ir}^{\text{IV}}-\text{O}\bullet$  and  $[\text{Ce}^{\text{IV}}(\text{NO}_3)_n\text{OH}]^{4-n-1}$  ( $n = 3$  and  $4$ ). Furthermore, pathways assisted by external water molecules were considered.<sup>38</sup> Before discussing the potential role of Ce in O–O bond formation, we revisited the well-accepted water nucleophilic attack<sup>39</sup> and interaction between two M–O moieties mechanisms.

O–O bond formation by direct reaction between two  $\text{L}_n\text{Ir}^{\text{IV}}-\text{O}\bullet$  moieties (SI)<sup>40</sup> is exergonic and has an activation barrier of 22.4 kcal/mol, while external water nucleophilic attack<sup>39</sup> at the  $\text{L}_n\text{Ir}^{\text{IV}}-\text{O}\bullet$  moiety has an activation barrier of 25.9 kcal/mol.<sup>41</sup> This is 3.5 kcal/mol higher than direct interaction between two  $\text{L}_n\text{Ir}^{\text{IV}}-\text{O}\bullet$  moieties, with the additional drawback that it is endergonic by 7.5 kcal/mol.

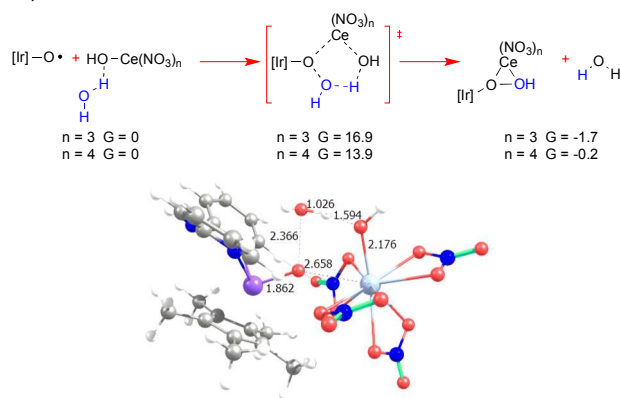




**Figure 3.** Schematic representation of O–O bond formation via nucleophilic attack of a water molecule to a  $L_nIr^{IV}-O\bullet$  moiety, assisted by  $[Ce^{IV}(NO_3)_4OH]^{-1}$  (top). Geometry of transition state for  $L_nIr^{IV}-O\bullet + [Ce^{IV}(NO_3)_4OH]^{-1}$  (bottom, distances in Å).

At this point we investigated the potential role of Ce species in O–O bond formation. Direct interaction of  $L_nIr^{IV}-O\bullet$  with  $[Ce^{IV}(NO_3)_nOH]^{4-n-1}$  ( $n = 3, 4$ ), reduces the energy barrier for O–O bond formation to roughly 16–20 kcal/mol. The transition state is characterized by an O–O distance of 1.75 Å and by an incipient interaction between the Ce atom and the O atom of the Ir moiety. The final product presents a strong interaction between Ce and the two O atoms of the formed O–O bond, see the SI. Interestingly, the reaction pathway with  $[Ce^{IV}(NO_3)_nOH]^{4-n-1}$  assisting nucleophilic attack of a water molecule to  $L_nIr^{IV}-O\bullet$  (Figure 3) has an even lower barrier, 14–16 kcal/mol, clearly lower than any barrier non assisted by Ce. It also has the advantage of being exergonic, thus driving thermodynamically O–O bond formation. The transition state geometry of Figure 3 illuminates the dual role of the Ce–OH moiety, with the Ce atom interacting with the O atom of  $L_nIr^{IV}-O\bullet$ , rendering it more electrophilic, and the OH moiety acting as proton acceptor from the water molecule performing the nucleophilic attack.

In conclusion, the kinetic results herein reported strongly suggest an alternative mechanism for WO driven by CAN in which, after an Ir catalyzed phase leading to the formation of a O–O bond containing moiety, the latter is transferred from Ir to an intermediate Ce-species that slowly liberates  $O_2$  without the intervention of the catalyst. DFT calculations show that CAN has a remarkable positive effect in the critical step of O–O bond formation. The proposed mechanism, deduced by investigating iridium WOCs but, in principle, of rather general validity, evidences once more, from an unprecedented perspective, the critical importance of multimetallic synergistic interactions in WOCs.

## ASSOCIATED CONTENT

**Supporting Information.** NMR characterization, catalytic experiments, computational details, and a CIF file giving crystallographic data. This material is available free of charge via the Internet at <http://pubs.acs.org>.

## AUTHOR INFORMATION

### Corresponding Author

\*Email: [luigi.cavallo@kaust.edu.sa](mailto:luigi.cavallo@kaust.edu.sa);  
[alceo.macchioni@unipg.it](mailto:alceo.macchioni@unipg.it)

## ACKNOWLEDGMENT

This work was financially supported by SABIC, Regione Umbria (POR FSE Projects), and COST Action CM1205 (CARISMA). We thank Prof. Antoni Llobet for helpful discussions and Dr. Stefano Giovagnoli for his help in performing DLS measurements.

## REFERENCES

(1) Balzani, V.; Credi, A.; Venturi, M. *ChemSusChem* **2008**, *1*, 26–58.

- (2) Young, K. J.; Martini, L. A.; Milot, R. L.; Snoeberger III, R. C.; Batista, V. S.; Schmuttenmaer, C. A.; Crabtree, R. H.; Brudvig, G. W. *Coord. Chem. Rev.* **2012**, *256*, 2503–2520.
- (3) For molecular catalysts, see: (a) *Molecular Water Oxidation*, Llobet, A., Ed., Wiley-Interscience: New York, 2014. (b) Kärkäs, M. D.; Verho, O.; Johnston, E. V.; Åkermark, B. *Chem. Rev.* **2014**, *114*, 11863–12001.
- (4) For catalysts based on inorganic materials see: Osterloh, F. E. *Chem. Mater.* **2008**, *20*, 35–54.
- (5) Renger, G. *Photosynth. Res.* **2007**, *92*, 407–425.
- (6) Parent, A. R.; Crabtree, R. H.; Brudvig, G. W. *Chem. Soc. Rev.* **2013**, *42*, 2247–2252.
- (7) Rongé, J.; Bosserez, T.; Martel, D.; Nervi, C.; Boarino, L.; Taulelle, F.; Decher, G.; Bordiga, S.; Martens, J. A. *Chem. Soc. Rev.* **2014**, *43*, 7963–7981.
- (8) Hara, M.; Waraksa, C. C.; Lean, J. T.; Lewis, B. A.; Mallouk, T. E. *J. Phys. Chem. A* **2000**, *104*, 5275–5280.
- (9) Yoshida, M.; Masaoka, S.; Abe, J.; Sakai, K. *Chem. Asian J.* **2010**, *5*, 2369–2378.
- (10) Wasylenko, D. J.; Ganesamoorthy, C.; Henderson, M. A.; Berlinguette, C. P. *Inorg. Chem.* **2011**, *50*, 3662–3672.
- (11) Kimoto, A.; Yamauchi, K.; Yoshida, M.; Masaoka, S.; Sakai, K. *Chem. Commun.* **2012**, *48*, 239–241.
- (12) Stull, J. A.; Britt, R. D.; McHale, J. L.; Knorr, F. J.; Lymar, S. V.; Hurst, J. K. *J. Am. Chem. Soc.* **2012**, *134*, 19973–19976.
- (13) Hettler, D. G. H.; Reek, J. N. H. *Eur. J. Inorg. Chem.* **2014**, 742–749.
- (14) Yoshida, M.; Kondo, M.; Torii, S.; Sakai, K.; Masaoka, S. *Angew. Chem. Int. Ed.* **2015**, *54*, 7981–7984.
- (15) Codolà, Z.; Gómez, L.; Kleespies, S. T.; Que, L., Jr.; Costas, M.; Lloret-Fillol, J. *Nat. Commun.* **2015**, *6*, 5865–5873.
- (16) (a) Savini, A.; Bellachioma, G.; Ciancaleoni, G.; Zuccaccia, C.; Zuccaccia, D.; Macchioni, A. *Chem. Commun.* **2010**, *46*, 9218–9219. (b) Savini, A.; Belanzoni, P.; Bellachioma, G.; Zuccaccia, C.; Zuccaccia, D.; Macchioni, A. *Green Chem.* **2011**, *13*, 3360–3374. (c) Bucci, A.; Savini, A.; Rocchigiani, L.; Zuccaccia, C.; Rizzato, S.; Albinati, A.; Llobet, A.; Macchioni, A. *Organometallics* **2012**, *31*, 8071–8074. (d) Savini, A.; Bucci, A.; Bellachioma, A.; Giancola, S.; Palomba, F.; Rocchigiani, L.; Rossi, A.; Suriani, A.; Zuccaccia, C.; Macchioni, A. *J. Organomet. Chem.* **2014**, *771*, 24–32; (e) Corbucci, I.; Petronilho, A.; Müller-Bunz, H.; Rocchigiani, L.; Albrecht, M.; Macchioni, A. *ACS Catal.* **2015**, *5*, 2714–2718.
- (17) Woods, J. A.; Bernhard, S.; Albrecht, M. in: *Molecular Water Oxidation*, Llobet, A., Ed., Wiley-Interscience: New York, 2014; pp 113–133.
- (18) Zuccaccia, C.; Bellachioma, G.; Bolaño, S.; Rocchigiani, L.; Savini, A.; Macchioni, A., *Eur. J. Inorg. Chem.* **2012**, 1462–1468.
- (19) Zuccaccia, C.; Bellachioma, G.; Bortolini, O.; Bucci, A.; Savini, A.; Macchioni, A. *Chem. Eur. J.* **2014**, *20*, 3446–3456.
- (20) Grotjahn, D. B.; Brown, D. B.; Martin, J. K.; Marelus, D. C.; Abadjian, M.-C.; Tran, H. N.; Kalyuzhny, G.; Vecchio, K. S.; Specht, Z. G.; Cortes-Llamas, S. A.; Miranda-Soto, V.; van, N. C.; Moore, C. E.; Rheingold, A. L. *J. Am. Chem. Soc.* **2011**, *133*, 19024–19027.
- (21) Koelewijn, J. M.; Lutz, M.; Dzik, W. I.; Detz, R. J.; Reek, J. N. H. *ACS Catal.* **2016**, *6*, 3418–3427.
- (22) Hong, D.; Murakami, M.; Yamada, Y.; Fukuzumi, S. *Energy Environ. Sci.* **2012**, *5*, 5708–5716. Contrary to what found by Fukuzumi, DLS measurements (SI) did not afford any indication of the presence of nanoparticles.
- (23) Samuni, A.; Czapski, G. *J. Chem. Soc. Dalton Trans.*, **1973**, 487–488 and references therein.
- (24) Wang, G.-C.; So, Y.-M.; Wong, K.-L.; Au-Yeung, K.-C.; Sung, H. H.-Y.; Williams, I. D.; Leung, W.-H. *Chem. Eur. J.* **2015**, *21*, 16126–16135.
- (25) Pook, N.-P.; Adam, A. Z. *Anorg. Allg. Chem.* **2014**, *640*, 2931–2938.

(26) Wang, G.-C.; Sung, H. H. Y.; Williams, I. D.; Leung, W.-H., *Inorg. Chem.* **2012**, *51*, 3640–3647.

(27) Coles, M. P.; Hitchcock, P. B.; Khvostov, A. V.; Lappert, M. F.; Li, Z.; Protchenko, A. V. *Dalton Trans.* **2010**, *39*, 6780–6788.

(28) Firouzabadi, H.; Iranpoor, N. *Synth. Commun.* **1984**, *14*, 875–882.

(29) Firouzabadi, H.; Iranpoor, N. Garzan, A. *Adv. Synth. Catal.* **2005**, *347*, 1925–1928.

(30) Paul, M.; Shirase, S.; Morimoto, Y.; Mathey, L.; Murugesapandian, B.; Tanaka, S.; Itoh, S.; Tsurugi, H.; Mashima, K. *Chem. Eur. J.* **2016**, *22*, 4008–4014

(31) Anandkumar, M.; Ramamurthy, C. H.; Thirunavukarasu, C.; Suresh Babu, K., *J. Mater. Sci.* **2015**, *50*, 2522–2531 and references therein.

(32) (a) Petronilho, A.; Rahman, M.; Woods, J. A.; Al-Sayyed, H.; Müller-Bunz, H.; MacElroy, J. M. D.; Bernhard, S.; Albrecht, M. *Dalton Trans.* **2012**, *41*, 13074–13080; (b) Hintermair, U.; Sheehan, S. W.; Parent, A. R.; Ess, D. H.; Richens, D. T.; Vaccaro, P. H.; Brudvig, G. W.; Crabtree, R. H. *J. Am. Chem. Soc.* **2013**, *135*, 10837–10851; (c) Woods, J. A.; Lalrempuia, R.; Petronilho, A.; McDaniel, N. D.; Müller-Bunz, H.; Albrecht, M.; Bernhard, S. *Energy Environ. Sci.* **2014**, *7*, 2316–2328.

(33) Lewandowska-Andralojc, A.; Polyansky, D. E.; Wang, C.-H.; Wang, W.-H.; Himeda, Y.; Fujita, E. *Phys. Chem. Chem. Phys.* **2014**, *16*, 11976–11987.

(34) Savini, A.; Bucci, A.; Bellachioma, G.; Rocchigiani, L.; Zuccaccia, C.; Llobet, A.; Macchioni A. *Eur. J. Inorg. Chem.* **2014**, 690–697.

(35) For a recent paper dealing with cerium oxide cluster ions capable of releasing oxygen see: Nagata, T.; Miyajima, K.; Mafuné, F. *J. Phys. Chem. A* **2015**, *119*, 1813–1819.

(36) Hintermair, U.; Hashmi, S. M.; Elimelech, M.; Crabtree, R. H. *J. Am. Chem. Soc.* **2012**, *134*, 9785–9795.

(37) Geometries were located with the Gaussian09 package at the BP86-D3 level using the SDD ECP on Ir and Ce and the SVP basis set on all main group atoms. Energies were refined by single-point calculations at the M06 level with the TZVP basis set on main group atoms. Solvent effects were included with the PCM approach. Full details, coordinates, absolute energies, and 3D view of all the computed species can be found in the SI.

(38) Chen, Z.; Concepcion, J. J.; Hu, X.; Yang, W.; Hoertz, P. G.; Meyer, T. J. *PNAS* **2010**, *107*, 7225–7229.

(39) Concepcion, J. J.; Tsai, M.-K.; Muckerman, J. T.; Meyer, T. J. *J. Am. Chem. Soc.* **2010**, *132*, 1545–1557.

(40) Richmond, C. J.; Sala, X.; Matheu, R.; Cavallo, L.; Poater, A.; Llobet, A.; Falivene, L.; Benet-Buccholz, J. *Chem. Eur. J.* **2014**, *20*, 17282–17286.

(41) Blakemore, J. D.; Schley, N. D.; Balcells, D.; Hull, J. F.; Olack, G. W.; Incarvito, C. D.; Eisenstein, O.; Brudvig, G. W.; Crabtree, R. H. *J. Am. Chem. Soc.* **2010**, *132*, 16017–16029

## FOR TABLE OF CONTENTS USE ONLY

